Daghigh Shirazi, Hamidreza; Håkansson, Karl M.O.; Abitbol, Tiffany; Vapaavuori, Jaana

A facile spinning approach towards the continuous production of aligned nanocellulose films

Published in:
Colloids and Surfaces A: Physicochemical and Engineering Aspects

DOI:
10.1016/j.colsurfa.2024.134673

Published: 20/11/2024

Document Version
Publisher's PDF, also known as Version of record

Colloids and Surfaces A: Physicochemical and Engineering Aspects 701 (2024) 134673

Contents lists available at ScienceDirect

Colloids and Surfaces A: Physicochemical and Engineering Aspects

journal homepage: www.elsevier.com/locate/colsurfa

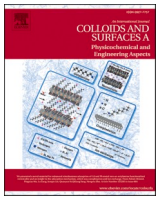

A facile spinning approach towards the continuous production of aligned nanocellulose films

Hamidreza Daghigh Shirazi [a], Karl M.O. Håkansson [b], Tiffany Abitbol [c], Jaana Vapaavuori [a,*]

[a] Department of Chemistry and Materials Science, Aalto University School of Chemical Engineering, Kemistintie 1, Espoo 02150, Finland
[b] RISE Research Institutes of Sweden , Drottning Kristinas väg 61, Stockholm SE-114 28, Sweden
[c] Institute of Materials, School of Engineering, EPFL, Lausanne 1015, Switzerland

HIGHLIGHTS

- A wet-spinning method to produce cellulose nanofibril (CNF) films is developed.
- The produced films demonstrate high light transmittance and partial CNF alignment.
- The CNF alignment provides an anisotropic humidity actuation.
- The wet-spinning approach has potential to continuous/scalable film production.

GRAPHICAL ABSTRACT

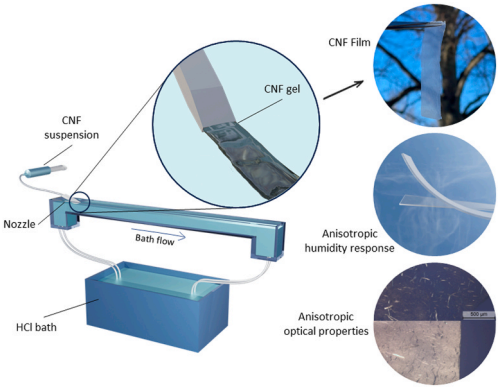

ARTICLE INFO

Keywords:
Cellulose nanofibril
CNF
Alignment
Optical transparency
Humidity actuation

ABSTRACT

In this work, we present an alternative approach to cellulose nanofibril film (CNF) production, taking inspiration from the wet spinning of fibers to wet spin films. During the spinning process, a CNF suspension is injected into a coagulation bath, where the partially aligned CNF network is locked. The CNF alignment of the dry films is then detected by wide angle X-ray scattering (WAXS). The comparison between the ultimate strengths and strengths at breaks of the films produced with different process parameters, including the suspension injection rate, bath pH, and bath flow rate, indicated no significant change in mechanical properties, suggesting a reliable and constant outcome for large-scale film fabrication. Furthermore, the produced films demonstrated high total light transmittance of 93 % at the wavelength of 550 nm, making them suitable for optoelectronic applications. Polarized optical microscopy revealed that even a low degree of CNF alignment can lead to anisotropic optical properties. Moreover, an anisotropic response to humidity was observed, in which the films preferentially bend in the perpendicular direction of the CNF orientation, thus opening a way for humidity-driven actuators.

* Corresponding author.
E-mail address: jaana.vapaavuori@aalto.fi (J. Vapaavuori).

https://doi.org/10.1016/j.colsurfa.2024.134673
Received 8 April 2024; Received in revised form 29 May 2024; Accepted 28 June 2024
Available online 20 July 2024

1. Introduction

Anisotropy, a distinctive feature observed in a range of natural materials, such as bones [1] and wood [2], brings about angular-dependency to material properties. In the case of wood, highly oriented cellulose nanofibrils (CNFs) provide the mechanical strength [3]. Zhu et al. [4] employed this inherent structure and produced anisotropic and transparent CNF films in a top-down approach, with potential green electronic applications. Their films exhibited a high fracture strength of ~350 MPa —15 times higher as compared to when measured in the direction perpendicular to CNF orientation — and optical transparency with a total light transmittance of ~90 % in the visible wavelength spectrum. Limitations posed by the dimensions of the films and non-continuous production process, however, highlight the need for alternatives to top-down approaches to fabricate such functional CNF films.

CNFs have a heterogeneous distribution of diameters, from a few nm up to bundles made up of 10–100 s of nm, and exhibit exceptional characteristics in terms of mechanical and optical properties [5–7]. Alignment of CNFs by external forces can be a way to approach their axisymmetric nanoscale characteristics within macroscale materials and achieve state-of-the-art materials with improved mechanical, optical, and swelling properties [8,9]. High alignment has been sought in different ways, for instance, by unidirectional stretching [10–12], and filament spinning [13]. The stretching approach consists of a step to increase the CNF concentration and form a hydrogel film, for instance by vacuum filtration, and then inducing the orientation using tensile testing machines. Besides the extensive sequence of steps, this approach faces inherent practical challenges in terms of the maximum strain of the hydrogel and process scalability. In filament wet spinning, the CNF suspension is injected through a nozzle into a coagulation bath [14–16]. The alignment can be achieved in three different processes: shear flow in the nozzle before coagulation, stretching (drawing) of the coagulated fiber, and shrinkage during drying. This alignment leads to improved mechanical strength of the fiber in the aligned direction [15]. The final properties are governed by several process parameters, such as concentration, injection rate, and nozzle geometry [17–19].

Nonetheless, CNF spinning processes have mainly focused on filament fabrication, and the feasibility of film production with a similar approach remains to be explored. This gains greater importance especially when the potential capabilities of such an approach are compared to approaches that are inflexible, energy-demanding, or limited to a small scale, e.g., restraint drying [11], magnetic and electric fields [20] and their coupling with mechanical stretching [21], and corona electric poling [22]. For instance, while the coupling of the magnetic and electric field achieved desirable mechanical properties, it required an intricate setup including a superconducting magnet to generate high magnetic fields and avoiding interference in the electric field producing system [20].

In this manuscript, we report a reproducible and straightforward method to continuously prepare anisotropic CNF films. Carboxymethylated CNFs go through a gel transition at a low pH due to charge screening and protonation of the surface charge which in turn promote increased interparticle interactions [23]. Thus, Hydrochloric acid (HCl) solutions at different pH were used as the coagulation bath with controlled flow rates, varying from 3 to 7 L min^{-1}. The feasibility of the process was investigated, and the mechanical and optical properties of the films and their anisotropic humidity actuation properties are presented. Furthermore, we discuss the influence of process parameters, namely, the CNF suspension injection rate, the HCl bath flow rate, and the pH of the bath. The results show that the proposed method is a promising choice for the fabrication of partially aligned CNF films without post treatment, having the potential for continuous and scalable production.

2. Results and discussion

Cellulose nanofibril (CNF) films were fabricated in a wet spinning process in which the CNF dispersion was injected through a submerged nozzle into a co-flowing coagulation bath, such that the dispersion underwent a gel transition in contact with the bath. The spinning setup is illustrated in Fig. 1a. The bath flow carries the formed gel film which is then collected to be dried in batches. During the drying process, the films are constrained in a custom frame to maintain their shape, ensure uniform drying, and prevent warping. It is noteworthy that continuous film fabrication can be enabled by using a winding collector for scale-up overcoming the slow pace of common CNF film fabrication processes [4,8–12]. Carboxymethyl groups on the CNF surfaces give rise to electrostatic repulsion and thus promote CNF dispersion in aqueous suspension [23]. The typical atomic force microscopy (AFM) height image of the CNF used in this work is presented in Fig. S1. A degree of substitution (DS) of 0.1 was selected as a standard charged grade for carboxymethylated CNF due to good fibrillation and colloidal stability. A lower DS could result in a loss of colloidal stability and inefficient fibrillation, leading to a reduced nanofraction yield and lower overall process efficiency. Conversely, a higher DS might decrease crystallinity by essentially polymerizing the surface chains. Furthermore, changing the CNF concentration may affect the processability and film formation, which will require further studies. We hypothesize that the shear stress exerted on the CNFs during the process leads to an alignment which is locked during the coagulation in a similar manner as presented by Håkansson (2021) [16]. As the CNF dispersion interacts with the HCl in the coagulation bath, HCl effectively reduces the electrostatic repulsion between the fibrils, enhancing cellulose-cellulose interactions. Therefore, the free-flowing CNF dispersion turns into a gel or a volume-spanning arrested state (VAS) [24]. In this state, the alignment of CNFs is locked and preserved in the final dried films.

Fig. 1b shows a representative photograph of a film successfully produced using the proposed wet spinning approach. SEM images displaying the surface morphology and cross-sectional view of this film are provided in Fig. S2. All films were produced using CNF suspensions at a constant concentration of 3.5 g L^{-1}. At lower concentrations, CNFs are more likely to be individually dispersed, facilitating better alignment during the spinning process, and therefore, improving the mechanical properties of the obtained films. In contrast, higher concentrations increase the proximity of the fibrils, leading to a higher probability of entanglement, which can hinder alignment during spinning. The alignment of the dried films was investigated using wide-angle X-ray scattering (WAXS). Fig. 1c-d shows the WAXS diffractograms of a wet-spun film as compared to a reference CNF film prepared by casting and submerging in the coagulation bath to directly go through a gel transition. As compared to the reference film which shows a uniform intensity distribution, an intensity variation along the crystal peak rings is observed for the spun film, indicating an increased uniaxial orientation along the machine direction. The corresponding azimuthal integration plot (Fig. 1d) compares the orientation distribution of the CNFs. While the reference film shows an almost flat orientation distribution, the spun film displays a lower minimum from which it is concluded that cellulose I crystals are more aligned in the machine direction (0°) in comparison to the cross direction (90°). Due to limitations of the WAXS equipment, the full 360° curve cannot be captured, however, because of double symmetry only 90° is needed for this analysis. The slight variation observed for the reference is attributed to the drying step. This is the only step that is not symmetric for the reference, since rectangular strips are produced and slight shrinkage in the cross direction upon drying was observed. Throughout this article, the samples are denoted by adopting a naming convention of X-Y-Z, in which X refers to pH, Y to injection rate (mL min^{-1}), and Z to bath flow rate (L min^{-1}).

Fig. 2 presents the normalized intensities at 90° (which is where the minimum intensities are found) from the WAXS curves of films and their ultimate tensile strength. The minimum intensity is used to quantify the

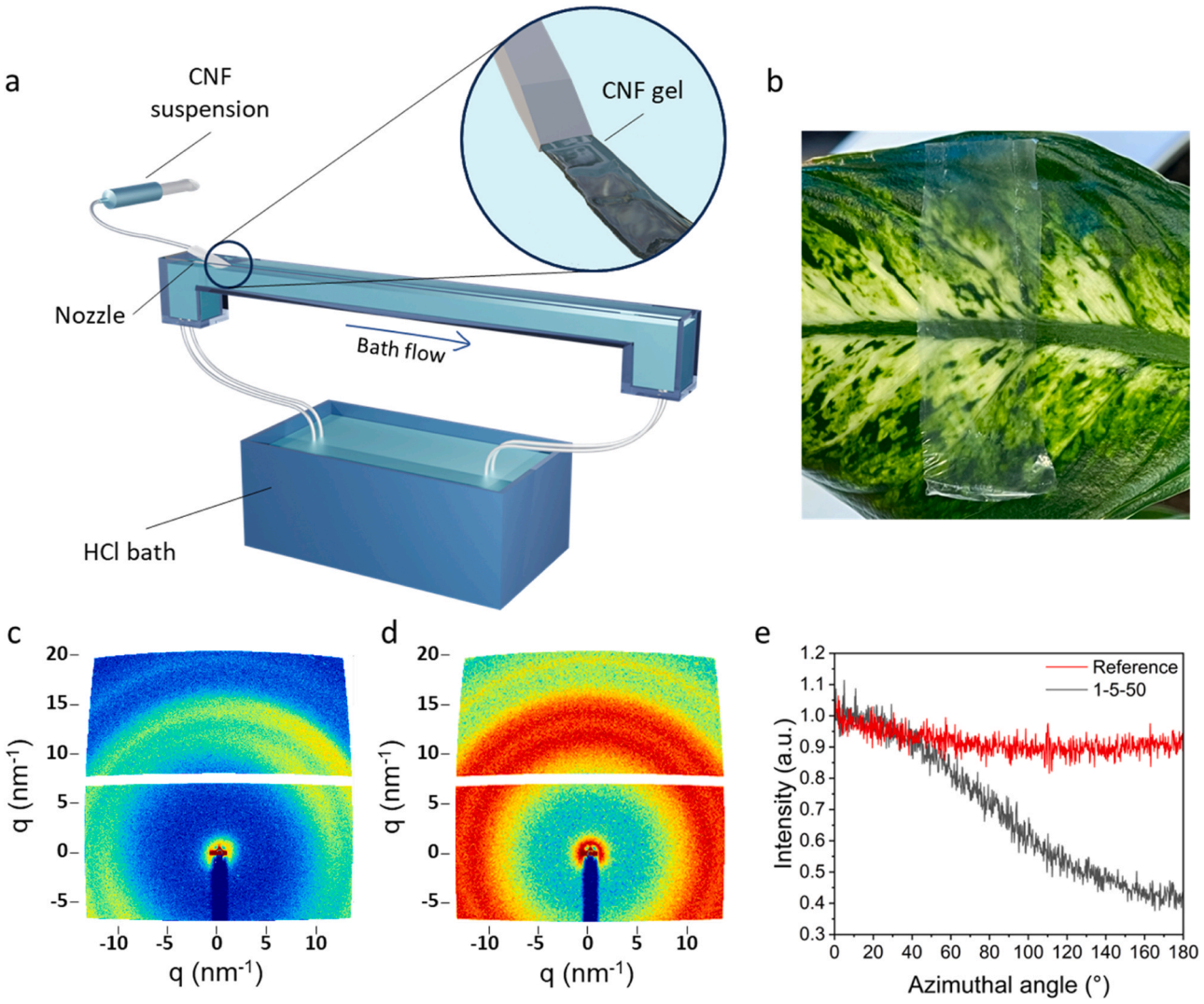

Fig. 1. a) Schematic presentation of the film fabrication process, in which the CNF suspension is injected into a flowing bath through a 20 mm wide nozzle, b) photograph of a produced film showcased against a leaf background to highlight its transparency, and WAXS diffractograms of c) spun (1−5−50), and d) reference films, and e) their azimuthal plot of the diffraction peak corresponding to the (200) crystal plane in cellulose I.

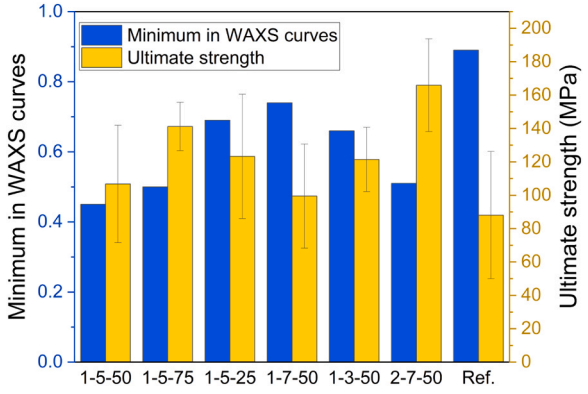

Fig. 2. The minimum intensities in WAXS curves and the ultimate tensile strength of films produced using different process parameters. The mean strength values and standard deviations are calculated based on at least four measurements.

CNF degree of alignment with a single value, where higher alignment leads to a lower minimum intensity. Other single value quantifications of the degree of alignment are used when a higher degree of alignment can be achieved, such as the order parameter and orientation parameter, f_c=*(180°-FWHM)/180°*. However, those are not suitable for our case since for example the orientation parameter would be $f_c = 0$ for all samples with a minimum larger than 0.5 (FWHM = 180°). Therefore, to show that there are differences in alignment, even if this alignment is small, the intensity minimum is used.

Overall, the spun films show a lower minimum in WAXS curves (from 0.45 to 0.84) as compared to the reference film (0.89), indicating partial CNF alignment stemming from the spinning process. Since no stretching of the films was involved in the process, and the drying method remained consistent across all samples, this suggests that the alignment results from the shear flow in the nozzle or the shear forces in the co-flowing coagulation bath. However, no clear trends can be identified with regards to the flow rates of the bath nor the CNF injection rate.

Evaluating the ultimate strength of the films confirms the robustness of the developed film fabrication method, in which the mechanical properties are immune to changing circumstances. Even though variations between mean values are seen, the variation within each sample is of the same order, which is similar magnitudes as in previous work [11,

12,16]. It can be observed that this range of alignments does not translate to any significant change in mechanical properties, as opposed to the top-down approach of Zhu et al [4]. The highest strength was recorded for the 2–7–50 film, measuring at 166 MPa, while the reference film showed the lowest at 88 MPa. Note that the 2–7–50 film was prepared from pH 2 coagulation bath and not from pH 1 as all other samples. Also noting that the strain at break is significantly larger compared to all other samples gives an indication that this sample is different in another way. It is known that HCl can induce hydrolysis of cellulose and it is hypothesized that this is the reason for the lower ultimate strength and lower strain at break for the pH 1 samples. Thus, low pH may also be the reason why the mechanical properties reported here are lower than in previous works [11,12,16].

Ultimate strengths of 123, 106, and 141 MPa were measured for 1–5–25, 1–5–50, and 1–5–75 films, indicating no discernible correlation between injection rates and the mechanical properties. Moreover, while the ultimate strengths of 1–3–50, 1–5–50, and 1–7–50 films hint at enhanced mechanical properties achieved by decreasing the bath flow rate, the overall values remain in the same range. Therefore, the small changes in the minimum in WAXS curves and similarity of the ultimate strengths suggest that the proposed film spinning method is capable of producing consistent properties, making it suitable for upscaling. Table 1 provides a detailed summary of the properties of the fabricated films. (The comparison of the strain at break and the modulus is visualized in Fig. S3, and the stress-strain curves of the films are presented in Fig. S4.)

Translucent CNF films can be great candidates for bio-based optoelectronics, such as substrates for solar cells and light-emitting diodes [25]. Fig. 3a-b compares the total light transmittance and haze of the 1–5–50 film, which showed the lowest minimum intensity, to that of the reference film (isotropic film). It is observed that the aligned film maintains a transmittance of over 90 % in the visible spectrum. The increase in transmittance and slightly lower haze of the aligned film could be attributed to a reduced number of scattering events along the path of light through the aligned film. This can be attributed to a slightly shorter light path length (~20 % thinner film) and perhaps also to fibril alignment, tentatively leading to a minor reduction of the density of scattering centers [26].

In Fig. 3c–e, polarized optical microscopy (POM) visualizes the birefringence of the films in between crossed polarizers, indicating the CNF orientation. The orientation of the CNF film's alignment director and the polarization axes are schematically illustrated in Fig. S5. The anisotropy of the aligned CNF film, including fiber fragments, allows polarized light to pass through the film when the average CNF orientation is at a 45° angle to the polarizers, causing the film to appear bright (Fig. S5a configuration). When the average CNF orientation is parallel to one of the polarizers, however, light transmission is minimized, resulting in the film appearing noticeably dark (Fig. S5b configuration). Alternatively, the POM images of the reference film (Fig. 3f-h) appear comparably dark and similar in different rotations, confirming the random CNF orientation.

In nature, many plants utilize a specific alignment of cellulose microfibrils to control their swelling and shrinking behavior [27]. For instance, in the case of pine cones [28], hygroscopic expansion of cells is governed by the orientation of CNFs in the cells, which enables a bending mechanism to release cone seeds. Similarly, the alignment of the studied CNF films leads to an anisotropic response to humidity. Upon exposure to humidity, elongation is restricted along the CNF alignment axis, promoting the winding motion in the cross direction. Video S1 displays such effect by simply placing the films near the surface of water. While a randomly oriented CNF film (isotropic film) shows low bending angles, a ribbon cut perpendicular to the spinning direction of 1–5–50 film bends in its length direction. Fig. 4 reports the bending angle of the ribbon as a function of time, in which the 1–5–50 ribbon with alignment perpendicular to its length achieves a maximum bending angle of ~20° in 5—6 s. In contrast, the ribbon cut in the spinning direction shows a near zero bending angle. The reference film, on the other hand, reaches a maximum of ~5°, highlighting how even small levels of alignment can influence the humidity actuation of CNF films. This actuating behavior has the potential to be used in a wide range of applications, including humidity sensors for environment control, soft robotics, and smart packaging [29,30].

Table 1
Properties of the CNF films.

	Minimum intensity in WAXS curve	Ultimate strength (MPa)	Modulus (GPa)	Strain at break (%)
1–3–50	0.66	121 ± 19	10.9 ± 1.2	1.4 ± 0.2
1–5–25	0.69	123 ± 37	12.4 ± 2.0	1.1 ± 0.3
1–5–50	0.45	107 ± 35	11.2 ± 1.1	1.2 ± 0.5
1–5–75	0.50	141 ± 2	10.5 ± 1.6	1.9 ± 0.2
1–7–25	0.84	127 ± 37	10.7 ± 2.6	1.5 ± 0.5
1–7–50	0.74	100 ± 31	9.6 ± 0.8	1.4 ± 0.6
1–7–75	0.63	127 ± 9	10.9 ± 1.0	1.6 ± 0.1
2–7–50	0.51	166 ± 28	10.1 ± 1.7	2.9 ± 0.7
Ref.	0.89	88 ± 17	9.9 ± 2.3	1.2 ± 0.6

3. Conclusion

A facile CNF film fabrication method was introduced, and the process parameters were investigated. The produced films show a slight alignment stemming from the process, which is hypothesized to arise from a combination of shear stresses in the nozzle and as the CNFs enter the co-flowing coagulation bath. Within this partial alignment range, no significant variation in the mechanical strengths of the spun films were observed. Therefore, we propose a robust method for producing partial alignment to CNF films without the hurdles related to the non-scalability of top-down techniques nor the batch-wise nature of employing a film stretching step. The partial CNF alignment achievable through this spinning method was sufficient to endow anisotropic functionalities to the films. The anisotropic alignment resulted in birefringence observable by polarized optical microscopy. Furthermore, it was particularly noticeable in the swelling of the film, imbuing an anisotropic response to humidity. Actuators with different humidity-induced bending modes could be produced by simply cutting film strips either parallel to or perpendicular to the average CNF alignment direction. The unique properties of these CNF films make them good candidates for flexible optical devices, sensors, and actuators. Furthermore, despite the continuous film formation, water removal and drying were done batch-wise. Therefore, developing an online drying method and enabling a roll-to-roll process will be the subject of future studies.

4. Experimental procedure

4.1. Materials

Cellulose nanofibrils (CNF) suspension was produced from a pulp (Dissolving Pulp Plus, Domsjö) that was carboxymethylated to a degree of substitution of 0.1, as previously described [31]. The pulp (0.4 wt%) was then microfluidized to generate the CNFs by high pressure homogenization using a M-110 EH microfluidizer from Microfluidics at 1700 bar for 4 passes. Poly(ethylene imine) (PEI) was purchased from Sigma-Aldrich and Mica discs from Ted Pella Inc.

4.2. Film fabrication

The CNF suspension with a concentration of 3.5 g/L is focused using a syringe pump (WPI, Al-4000) to a nozzle submerged in the flowing HCl bath (Fig. 1a). The nozzle tip has a dimension of 2 mm × 20 mm. The injection rate was controlled by the syringe pump and the bath flow was monitored using a flow meter. CNF suspension was injected with volumetric flow rate of 25, 50, and 75 mL min^{-1} into the HCl bath (pH 1 and

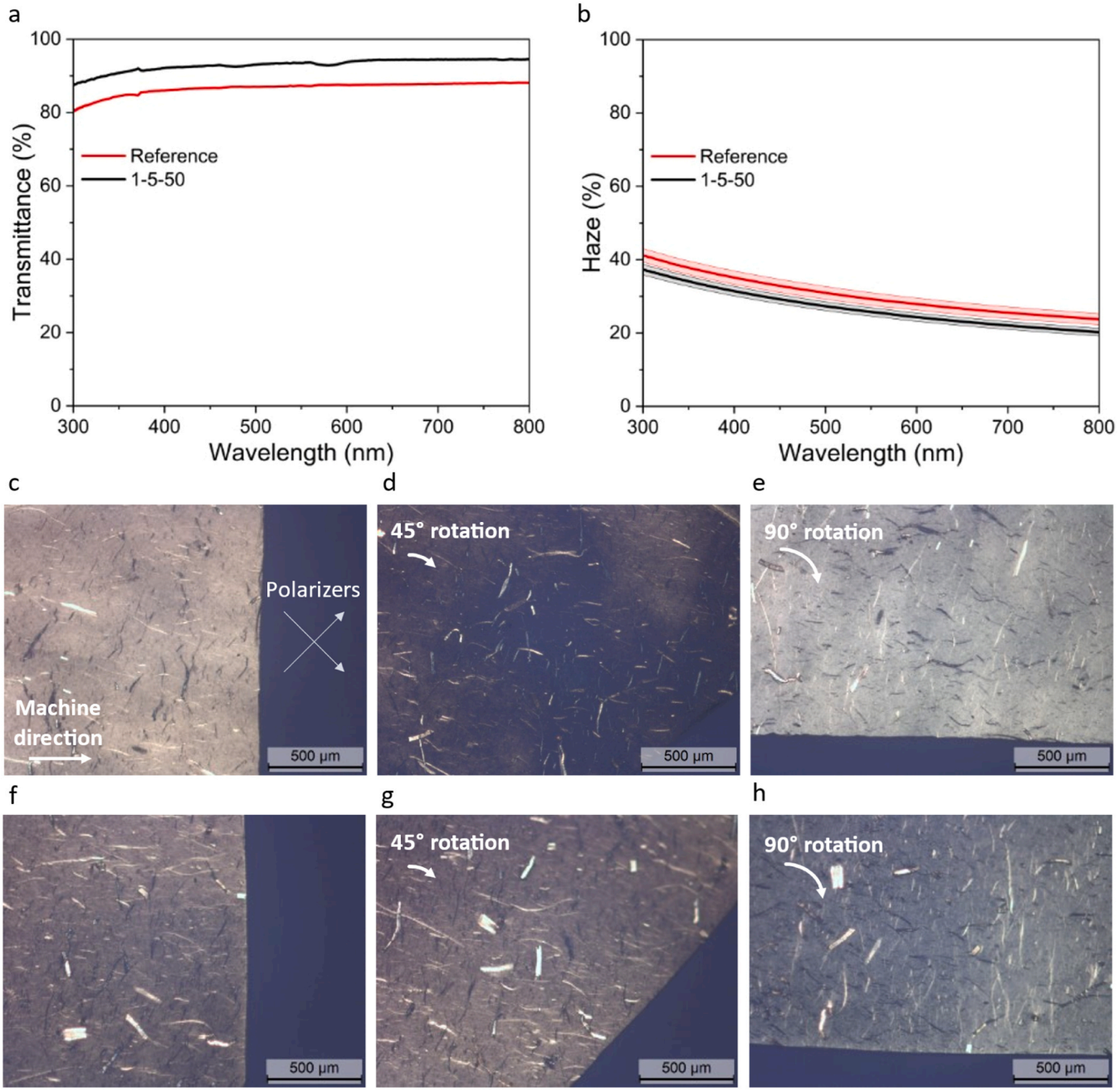

Fig. 3. a) Total light transmittance and b) haze of the aligned (1−5−50) and isotropic films (the lines and bands represent the mean values and standard deviations of three measurements). The polarized optical microscopy images of the c-e) 1–5–50, and f-h) reference films at different rotations.

2) with flow rate of 3, 5, and 7 L min^{-1}. A polymer mesh was placed on the bottom of the bath and was used to lift and transfer the CNF gel. The gels were then cut in 20 cm long pieces, placed on Durapore Membrane filters (Merck, Ireland) and the edges were constrained to prevent wrinkles. The CNF gels were then dried at 25 °C and 50 % humidity. The reference film was produced by casting the CNF suspension on a flat surface and dipping it in the coagulation bath at once to go through the gel transition. The gel was then cut and dried similar to the spun films.

4.3. Wide-angle X-ray spectroscopy (WAXS)

The Wide-Angle X-ray Scattering (WAXS) was performed on the same system as previously described [16]. In short, an Anton Paar SAXSPoint 2.0 system (Anton Paar, Graz, Austria) was used, having a Microsource X-ray source providing a wavelength of 0.15418 nm with by CuKa radiation. The detector was a Dectris 2D CMOS Eigher R 1 M with a pixel size of 75 µm by 75 µm. The beamsize was approximately 500 µm in diameter and the sample to detector distance was 111 mm. The exposure time was 13 h in total by 26 frames with each frame taking 30 minutes to complete. The transmittance was measured for all samples and used in the normalization of the data, which was performed with the SAXSanalysis 3.00.042 (Anton Paar, Graz, Austria) software and MATLAB (Mathworks).

4.4. Tensile testing of films

The tensile properties of the films were measured with an MTS tensile tester in combination with a Teststar ISS controller (MTS Systems Corp., USA). The films were conditioned at 50 % RH and 23 °C for one week prior to the tests in the same environment as the tests were

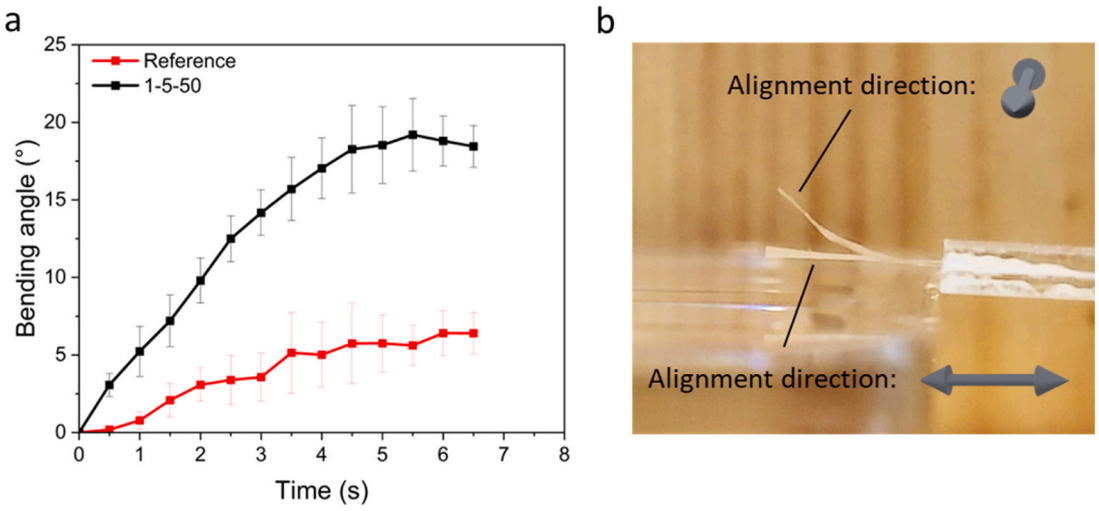

Fig. 4. a) Bending angles of CNF strips over time, where the alignment of the 1–5–50 film is perpendicular to the CNF ribbon length, and b) a representative photograph, comparing the bending behavior of 1–5–50 strips with different alignment directions.

performed. Test specimens were cut in a rectangular shape with a length of 45 mm and a width of 6 mm, and their thicknesses were measured using a digital caliper. The gap distance was 30 mm, and the speed was set to 0.5 mm/s. Seven specimens per sample were measured.

4.5. Polarized optical microscopy (POM)

The orientation distribution of fibrils was visualized by placing the films in between two glass slides to flatten possible wrinkles. The characterization was performed by using a Leica 1090 optical microscope under cross-polarized light.

4.6. UV–visible spectrophotometry

The optical properties of the films were measured using UV-2600 with ISR-2600Plus integrating sphere attachment, Shimadzu, Japan in the range of 300 – 800 nm. The total light transmittance and haze were calculated using the following equations and the average of 3 measurements was reported:

$$\text{Transmittance}(\%) = \frac{T_2}{T_1} \times 100 \quad (2)$$

$$\text{Haze}(\%) = \left(\frac{T_4}{T_2} - \frac{T_3}{T_1}\right) \times 100 \quad (3)$$

where T_1 is the transmission of light without the sample (as reference), T_2 is the transmitted light through the sample, T_3 is the scattering of light by the device without the sample, and T_4 is the diffusive transmittance.

4.7. Humidity actuation test

The films were cut in strips of approximately 2 mm × 10 mm in cross-directions. The strips were then clamped and placed adjacent to the water surface, and the process was recorded using Sony IMX586 48-megapixel sensor. The corresponding bending angles were extracted manually by image analysis using ImageJ software (version 1.53e, National Institutes of Health, USA).

4.8. Scanning electron microscopy (SEM)

The samples were first sputter-coated with a 5 nm Au/Pd layer (80/20) and then analyzed using Tescan Mira3 scanning electron microscope (SEM).

4.9. Atomic force microscopy (AFM)

Mica substrates were first dipped in a Poly(ethylene imine) (PEI, 2.5 %) solution for 1 min and then carefully rinsed with water. The CNF suspension was diluted to 0.001 wt%, and a 10 μL droplet was placed on the mica substrate and allowed to dry at room temperature. AFM was performed using multimode 8 AFM with Nanoscope V controller (Bruker, Santa Barbara, CA) in tapping mode with non-contact AFM cantilevers (NCHV-A, 8 nm tip radius, Bruker).

CRediT authorship contribution statement

Karl M.O. Håkansson: Writing – review & editing, Validation, Supervision, Resources, Methodology, Investigation, Formal analysis, Conceptualization. **Hamidreza Daghigh Shirazi:** Writing – review & editing, Writing – original draft, Investigation, Formal analysis, Data curation, Conceptualization, Funding acquisition. **Jaana Vapaavuori:** Writing – review & editing, Validation, Supervision, Project administration, Methodology, Funding acquisition, Formal analysis, Conceptualization. **Tiffany Abitbol:** Writing – review & editing, Validation, Supervision, Project administration, Methodology, Funding acquisition, Formal analysis, Data curation, Conceptualization.

Declaration of Competing Interest

The authors declare that they have no known competing financial interests or personal relationships that could have appeared to influence the work reported in this paper.

Data availability

Data will be made available on request.

Acknowledgements

This work was financially supported and part of the Academy of Finland's Flagship Program under Projects No. 318890 and 318891 (Competence Center for Materials Bioeconomy, FinnCERES). Bio-Economy and RaMi infrastructures were employed in this work. Karl Håkansson kindly acknowledge the financial support from the Nils and Dorthi Troedsson Research fund. T.A. acknowledges the Chair in Sustainable Materials at EPFL, co-funded by BASF, Logitech, Nestlé, and SIG. Dr. Hoang M. Nguyen is acknowledged for his help in acquiring the AFM images.

Appendix A. Supporting information

Supplementary data associated with this article can be found in the online version at doi:10.1016/j.colsurfa.2024.134673.

References

[1] S. Weiner, W. Traub, H.D. Wagner, Lamellar bone: structure–function relations, J. Struct. Biol. 126 (3) (1999) 241–255, https://doi.org/10.1006/jsbi.1999.4107.

[2] Ethington R.L., Hilbrand H.C. Anisotropy in Wood. In: Fifth Pacific Area National Meeting of the Society. ASTM International; 1966:21-21-18. doi:10.1520/STP45149S.

[3] S. Ling, D.L. Kaplan, M.J. Buehler, Nanofibrils in nature and materials engineering, Nat. Rev. Mater. 3 (4) (2018) 18016, https://doi.org/10.1038/natrevmats.2018.16.

[4] M. Zhu, Y. Wang, S. Zhu, et al., Anisotropic, transparent films with aligned cellulose nanofibers, Adv. Mater. 29 (21) (2017) 1606284, https://doi.org/10.1002/adma.201606284.

[5] L. Zhai, H.C. Kim, J.W. Kim, J. Kang, J. Kim, Elastic moduli of cellulose nanofibers isolated from various cellulose resources by using aqueous counter collision, Cellulose 25 (7) (2018) 4261–4268, https://doi.org/10.1007/s10570-018-1836-x.

[6] A. Kafy, H.C. Kim, L. Zhai, et al., Cellulose long fibers fabricated from cellulose nanofibers and its strong and tough characteristics, Sci. Rep. 7 (1) (2017) 17683, https://doi.org/10.1038/s41598-017-17713-3.

[7] Y. Zhang, T. Nypelö, C. Salas, J. Arboleda, I.C. Hoeger, O.J. Rojas, Cellulose nanofibrils, J. Renew. Mater. 1 (3) (2013) 195–211, https://doi.org/10.7569/JRM.2013.634115.

[8] K. De France, Z. Zeng, T. Wu, G. Nyström, Functional materials from nanocellulose: utilizing structure–property relationships in bottom-up fabrication, Adv. Mater. 33 (28) (2021) 2000657, https://doi.org/10.1002/adma.202000657.

[9] K. Li, C.M. Clarkson, L. Wang, et al., Alignment of cellulose nanofibers: harnessing nanoscale properties to macroscale benefits, ACS Nano 15 (3) (2021) 3646–3673, https://doi.org/10.1021/acsnano.0c07613.

[10] G. Josefsson, P. Ahvenainen, N.E. Mushi, E.K. Gamstedt, Fibril orientation redistribution induced by stretching of cellulose nanofibril hydrogels, J. Appl. Phys. 117 (21) (2015), https://doi.org/10.1063/1.4922038.

[11] C. Baez, J. Considine, R. Rowlands, Influence of drying restraint on physical and mechanical properties of nanofibrillated cellulose films, Cellulose 21 (1) (2014) 347–356, https://doi.org/10.1007/s10570-013-0159-1.

[12] H. Sehaqui, N. Ezekiel Mushi, S. Morimune, M. Salajkova, T. Nishino, L. A. Berglund, Cellulose nanofiber orientation in nanopaper and nanocomposites by cold drawing, ACS Appl. Mater. Interfaces 4 (2) (2012) 1043–1049, https://doi.org/10.1021/am2016766.

[13] K.M.O. Håkansson, A.B. Fall, F. Lundell, et al., Hydrodynamic alignment and assembly of nanofibrils resulting in strong cellulose filaments, Nat. Commun. 5 (1) (2014) 4018, https://doi.org/10.1038/ncomms5018.

[14] A. Walther, J.V.I. Timonen, I. Díez, A. Laukkanen, O. Ikkala, Multifunctional high-performance biofibers based on wet-extrusion of renewable native cellulose nanofibrils, Adv. Mater. 23 (26) (2011) 2924–2928, https://doi.org/10.1002/adma.201100580.

[15] S. Iwamoto, A. Isogai, T. Iwata, Structure and mechanical properties of wet-spun fibers made from natural cellulose nanofibers, Biomacromolecules 12 (3) (2011) 831–836, https://doi.org/10.1021/bm101510r.

[16] K.M.O. Håkansson, Effect of carboxymethylated cellulose nanofibril concentration regime upon material forming on mechanical properties in films and filaments, Cellulose 28 (2) (2021) 881–895, https://doi.org/10.1007/s10570-020-03566-z.

[17] M.J. Lundahl, V. Klar, L. Wang, M. Ago, O.J. Rojas, Spinning of cellulose nanofibrils into filaments: a review, Ind. Eng. Chem. Res 56 (1) (2017) 8–19, https://doi.org/10.1021/acs.iecr.6b04010.

[18] T. Rosén, B.S. Hsiao, L.D. Söderberg, Elucidating the opportunities and challenges for nanocellulose spinning, Adv. Mater. 33 (28) (2021), https://doi.org/10.1002/adma.202001238.

[19] N. Mittal, F. Ansari, K. Gowda.V, et al., Multiscale control of nanocellulose assembly: transferring remarkable nanoscale fibril mechanics to macroscale fibers, ACS Nano 12 (7) (2018) 6378–6388, https://doi.org/10.1021/acsnano.8b01084.

[20] H.C. Kim, J.W. Kim, L. Zhai, J. Kim, Strong and tough long cellulose fibers made by aligning cellulose nanofibers under magnetic and electric fields, Cellulose 26 (10) (2019) 5821–5829, https://doi.org/10.1007/s10570-019-02496-9.

[21] S. Yun, S. Jang, G.Y. Yun, J. Kim, Electrically aligned cellulose film for electro-active paper and its piezoelectricity, Smart Mater. Struct. 18 (11) (2009) 117001, https://doi.org/10.1088/0964-1726/18/11/117001.

[22] S. Yun, J.H. Kim, Y. Li, J. Kim, Alignment of cellulose chains of regenerated cellulose by corona poling and its piezoelectricity, J. Appl. Phys. 103 (8) (2008) 083301, https://doi.org/10.1063/1.2908883.

[23] A.B. Fall, S.B. Lindström, O. Sundman, L. Ödberg, L. Wågberg, Colloidal stability of aqueous nanofibrillated cellulose dispersions, Langmuir 27 (18) (2011) 11332–11338, https://doi.org/10.1021/la201947x.

[24] M. Nordenström, A. Fall, G. Nyström, L. Wågberg, Formation of colloidal nanocellulose glasses and gels, Langmuir 33 (38) (2017) 9772–9780, https://doi.org/10.1021/acs.langmuir.7b01832.

[25] J.J. Kaschuk, Y. Al Haj, O.J. Rojas, K. Miettunen, T. Abitbol, J. Vapaavuori, Plant-based structures as an opportunity to engineer optical functions in next-generation light management, Adv. Mater. 34 (6) (2022), https://doi.org/10.1002/adma.202104473.

[26] J.J. Kaschuk, Y. Al Haj, J. Valdez Garcia, et al., Processing factors affecting roughness, optical and mechanical properties of nanocellulose films for optoelectronics, Carbohydr. Polym. 332 (2024) 121877, https://doi.org/10.1016/j.carbpol.2024.121877.

[27] R.M. Erb, J.S. Sander, R. Grisch, A.R. Studart, Self-shaping composites with programmable bioinspired microstructures, Nat. Commun. 4 (1) (2013) 1712, https://doi.org/10.1038/ncomms2666.

[28] C. Dawson, J.F.V. Vincent, A.M. Rocca, How pine cones open, 668-668, Nature 390 (6661) (1997), https://doi.org/10.1038/37745.

[29] G. Ayissi Eyebe, B. Bideau, N. Boubekeur, É. Loranger, F. Domingue, Environmentally-friendly cellulose nanofibre sheets for humidity sensing in microwave frequencies, Sens Actuators B Chem. 245 (2017) 484–492, https://doi.org/10.1016/j.snb.2017.01.130.

[30] S. Taccola, F. Greco, E. Sinibaldi, A. Mondini, B. Mazzolai, V. Mattoli, Toward a new generation of electrically controllable hygromorphic soft actuators, Adv. Mater. 27 (10) (2015) 1668–1675, https://doi.org/10.1002/adma.201404772.

[31] L. Wågberg, G. Decher, M. Norgren, T. Lindström, M. Ankerfors, K. Axnäs, The build-up of polyelectrolyte multilayers of microfibrillated cellulose and cationic polyelectrolytes, Langmuir 24 (3) (2008) 784–795, https://doi.org/10.1021/la702481v.